Structural Refinement of Titanium-Aluminum-Niobium Alloy for Biomedical Applications

Joaquín E. González-Hernández[1], Jorge M. Cubero-Sesin[1,2]*, Elena Ulate-Kolitsky[1], Priscilla Navarro[1], Stephen Petretti[1] and Zenji Horita[3,4]

[1]*School of Materials Science and Engineering, Costa Rica Institute of Technology, Cartago 159-7050, Costa Rica*
[2]*Institutional Microscopy Laboratory, Costa Rica Institute of Technology, Cartago 159-7050, Costa Rica*
[3]*Department of Materials Science and Engineering, Kyushu University, Fukuoka 819-0395, Japan*
[4]*WPI, International Institute of Carbon-Neutral Energy Research (WPI-I2CNER), Kyushu University, Fukuoka 819-0395, Japan*

Received November 25, 2016; Accepted February 17, 2017

ABSTRACT: In this work, a modification of the microstructure of a commercial Ti-6Al-7Nb alloy was accomplished by high-pressure torsion (HPT) at room temperature, to produce a bulk nanostructure on discs of 10 mm diameter and ~0.8 mm thickness. The metallographic analyses of the discs were performed by optical microscopy and scanning electron microscopy with energy dispersive spectroscopy. The results confirmed the presence of aluminum (Al) and niobium (Nb) as the sole alloying elements, promoting a duplex (α + β) titanium (Ti) microstructure prior to HPT processing. After HPT processing, nanostructure refinement was attained, reflected in the X-ray diffraction profiles as broadening of the α-Ti and β-Ti peaks and the appearance of the ω-Ti phase. Transmission electron microscopy confirmed a grain size < 100 nm after HPT processing for N = 5 revolutions. Microhardness increased significantly with straining by HPT, which can be attributed both to the grain refinement and the formation of the ω-Ti phase.

KEYWORDS: Titanium-aluminum-niobium, omega (ω-Ti) phase, high-pressure torsion, nanostructure, solid-state transformation

1 INTRODUCTION

Because of a good combination of corrosion resistance, mechanical strength, biocompatibility and moderate Young's modulus, Ti-6Al-4V alloy is one of the most popular metallic biomaterials in orthopedics. These properties have established this alloy as a preferred material for orthopedic implants, as well as other medical devices, such as artificial hip and dental implants, for several decades [1–4]. However, it has been shown that the release of V^+ ions in concentrations above 10 μg/ml is cytotoxic for tissues near an implant. More recently, new alloy designs have been proposed using Nb as replacement for V^+ [5–6]. Niobium does not produce this harmful effect, but rather is considered a vital element. Good compatibility with real bone and biocompatibility has been observed using a honeycomb structure of Ti-6Al-7Nb [7, 8]. These designs of Ti-6Al-7Nb alloys have a similar duplex (α + β) structure and mechanical properties equivalent to Ti-6Al-4V alloys, with a lower risk of cytotoxicity [9, 10]. Two characteristic phases have been identified experimentally for this kind of duplex Ti alloy at room/ambient temperature and pressure: an alpha (α-Ti) phase with a hexagonal close packed (HCP) crystal structure, and a high temperature beta (β-Ti) phase with a body-centered cubic (BCC) crystal structure. Both phases can coexist at room temperature due to the presence of α-Ti and β-Ti phase stabilizers such as Al and Nb, respectively. The maximum solubility of Nb in the α-Ti matrix is 2.2 ± 0.5 at%. Concentrations of Nb above this value result in the appearance of the β phase leading to the α + β two-phase region [11–13]. The α + β duplex structure provides these alloys with an appropriate combination of strength and ductility, which may be ideal for applications such as implants and other medical devices [14, 15].

Besides the transformation of α-Ti to β-Ti crystal structure at high temperature, the similar allotropic phase transformation occurs from the α-Ti phase to the omega (ω-Ti) phase by application of high

*Corresponding author: jcubero@itcr.ac.cr

DOI: 10.7569/JRM.2017.634120

pressure in Ti and Ti-based alloys. The ω-Ti phase has been observed above 5 GPa at room temperature and it is said to be metastable after the pressure is released [16]. The ω-Ti phase has had positive and negative implications for application in the aerospace industry because the ω-Ti phase can precipitate during aging treatments, and while it decreases the toughness and ductility of Ti alloys, particularly of β-Ti alloys, it has been shown to retard fatigue crack growth [17]. Nevertheless, no study has been available for investigating the possibility to nucleate and disperse fine particles of this ω-Ti phase uniformly in the duplex matrix.

Severe plastic deformation (SPD) methods, such as high-pressure torsion (HPT), have been shown to enhance the mechanical properties of bulk metallic materials, due to the significant grain refinement of conventional pure metals and alloys down to nanosizes [18, 19]. Figure 1 shows a schematic illustration of the HPT facility where high pressure and torsional strain can be applied concurrently on a disc sample using upper and lower anvils that can rotate with respect to each other [20].

High-pressure torsion processing allows processing of Ti-based alloys, such as Ti-6Al-4V and Ti-6Al-7Nb, to achieve grain refinement and enhance their mechanical properties such as microhardness and superplasticity [6, 21]. Also, the formation of ω-Ti phase has been observed during HPT processing of commercial purity Ti at pressures > 4 GPa [22] and in Ti-6Al-7Nb at 6 GPa [1]. Thus, the aim of this work is to study the effect of intense torsional strain on the phase composition and the microhardness of a commercial Ti-6Al-7Nb alloy using the HPT technique in order to evaluate the microstructure evolution and the degree of nanostructuring.

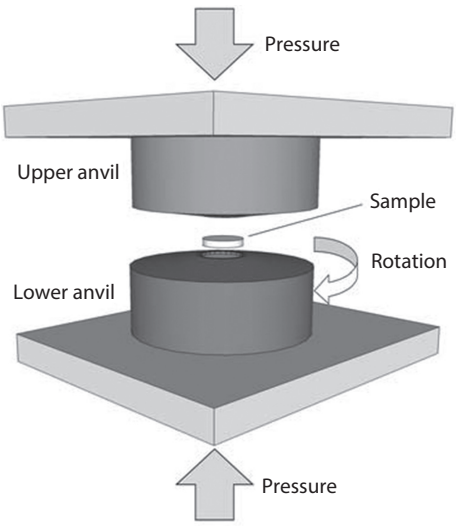

Figure 1 Schematic diagram of high-pressure torsion (HPT) technique.

2 EXPERIMENTAL PROCEDURES

A set of 10 mm discs with a thickness of ~1 mm was sliced from a commercial rod of Ti-6Al-7Nb by electrical discharge machining (EDM). After grinding both sides of the discs to remove the surface oxidized layers, they were placed between the anvils of the HPT facility as shown in Figure 1. The discs were processed at room temperature under an applied pressure of 6 GPa with a rotation speed of 1 rpm for N = 1, 5 and 15 revolutions. After HPT processing, the thickness of the discs was ~0.8 mm.

The HPT processed discs were prepared for metallographic analysis and Vickers microhardness measurements (Mitutoyo HM-101 durometer). For this purpose, the surface was further ground mechanically with waterproof emery papers from 500 up to 4000 grit and then polished to a mirror-like surface using an alumina suspension containing 0.3 μm particle size. Microhardness indentations were performed in 12 radial directions from the center of the discs with a 500 μm spacing using a load of 0.2 kgf for 15 s. To reveal the phase composition and the grain sizes, the samples were etched with 10% $HF_{(ac)}$ as chemical reagent. The overall metallographic observations on the etched surfaces of the discs were performed by optical microscopy (OM) at several distances from the center of the discs. To obtain more detail in the phase morphology, scanning electron microscopy (SEM) images of the sample surfaces were obtained using a Hitachi TM-1000 tabletop microscope at an acceleration voltage of 15 kV. The chemical composition of the alloy was also verified with energy dispersive spectroscopy (EDS) during the SEM observations.

Further microstructural studies were carried out by X-ray diffraction (XRD) using a PANalytical Empyrean diffractometer with Cu-Kα (λ = 1,54016 Å) radiation. Scans were performed in the range of 2θ = 30°–90° with a scan step of 0.003° and a scan speed of 45 s/step. The microstructure of the HPT-processed sample for N = 5 revolutions was observed by transmission electron microscopy (TEM) using a JEOL JEM-2100 microscope with an acceleration voltage of 200 kV. For this purpose, a 3 mm disc was punched out from the disc and ground with waterproof emery papers (2000 grit) down to a thickness of 0.2 mm. The disc was further thinned to electron transparency by twin-jet electropolishing at 18 °C, using a solution of 90% acetic acid and 10% perchloric acid under an applied voltage of 20 V. Selected area electron diffraction (SAED) patterns

were recorded from an area ~1 μm in diameter, and images were recorded in bright- and dark-field modes.

3 RESULTS AND DISCUSSION

Figure 2 shows an EDS profile after HPT processing for N=5 revolutions. The characteristic X-ray radiation peaks of Ti, Al and Nb were identified and labeled accordingly in the spectrum. The quantitative analysis revealed a composition of 7.1% Al, 7.1% Nb and 85.9% Ti, which is within the specification of this alloy. No major impurities were detected. The presence of these alloying elements in Ti promotes the presence of a two-phase, or duplex (α + β) crystal structure, as it is known for Ti-6Al-7Nb [23, 24]. Since Al is an α-Ti (equilibrium) phase stabilizing element, and Nb is a β-Ti (high temperature) phase stabilizing element, both phases can coexist at room temperature and ambient pressure conditions [25]. The EDS results confirm no major impurities or contamination of the specimen occurred because of HPT processing, which is an important characteristic of this process [18].

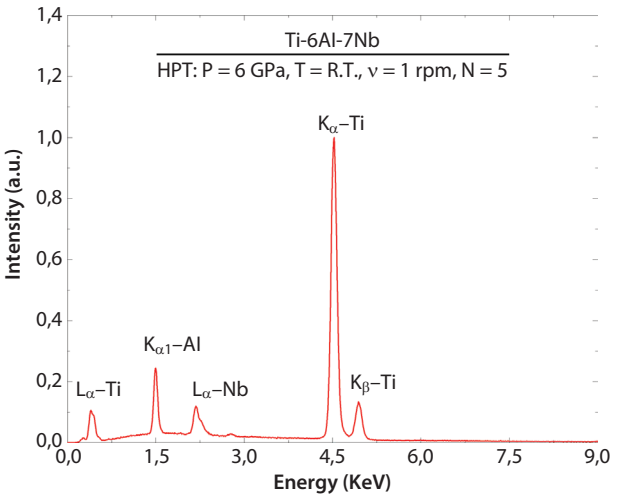

Figure 2 Energy dispersive spectroscopy (EDS) profile of Ti-6Al-7Nb sample processed by HPT for N = 5 revolutions.

Figure 3 shows the microstructure of the alloy in the condition prior to the HPT processing. Figure 3a corresponds to an OM micrograph where a two-phase structure can be z`appreciated from the image but the morphology of individual crystals is difficult to resolve at low magnification. Figure 3b corresponds to a backscattered electron image from an enlarged region of the sample in Figure 3a. Thus, the phase contrast in SEM is inverted with respect to the OM micrograph, which allows appreciating that the microstructure of the α-Ti phase is composed of equiaxed micron-sized grain structure and particles of the β-Ti phase with 1–3 μm size [1]. The magnified region in Figure 3c shows that the β-Ti particles are mostly present in the grain boundaries of the α-Ti phase, and some particles within the grains were observed. This is due to the nucleation of some α grains from β particles suspended in the melt during the casting process.

Figure 4 shows SEM images of the microstructures after HPT processing. Figure 4a is from a sample processed for N = 1 revolutions, while Figure 4b is from a sample processed for N = 5 revolutions and Figure 4c is from a sample processed for N = 15 revolutions. The microstructure shown in Figure 4a shows that after N=1 revolutions the structure has not been altered much from the condition prior to HPT shown in Figure 3c. On the other hand, in Figure 4b, the development of a preferred orientation can be appreciated in some regions after N = 5 revolutions by the elongation of β-phase shown in bright contrast. However, in the image shown in Figure 4c, which was recorded at higher magnification, such preferred orientation of the crystals is not so clear, which supposes that a more homogeneous deformation of the

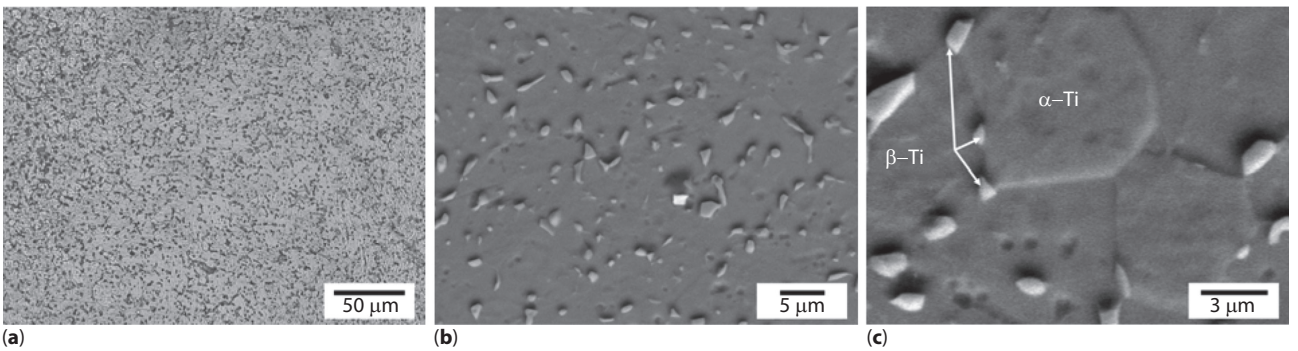

Figure 3 Micrographs of Ti-6Al-7Nb prior to HPT processing: (**a**) optical microscopy and (**b**,**c**) scanning electron microscopy.

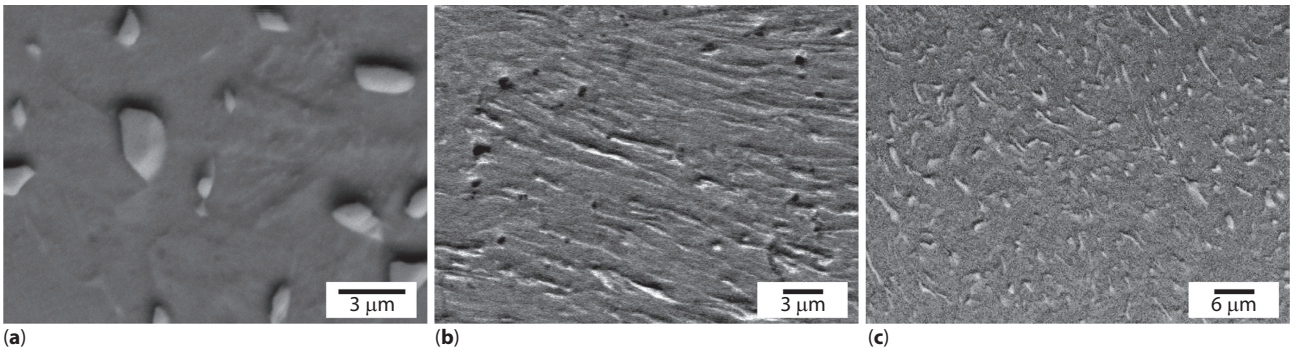

Figure 4 SEM images of Ti-6Al-7Nb after HPT processing for (**a**) N = 1, (**b**) N = 5 and (**c**) N = 15 revolutions.

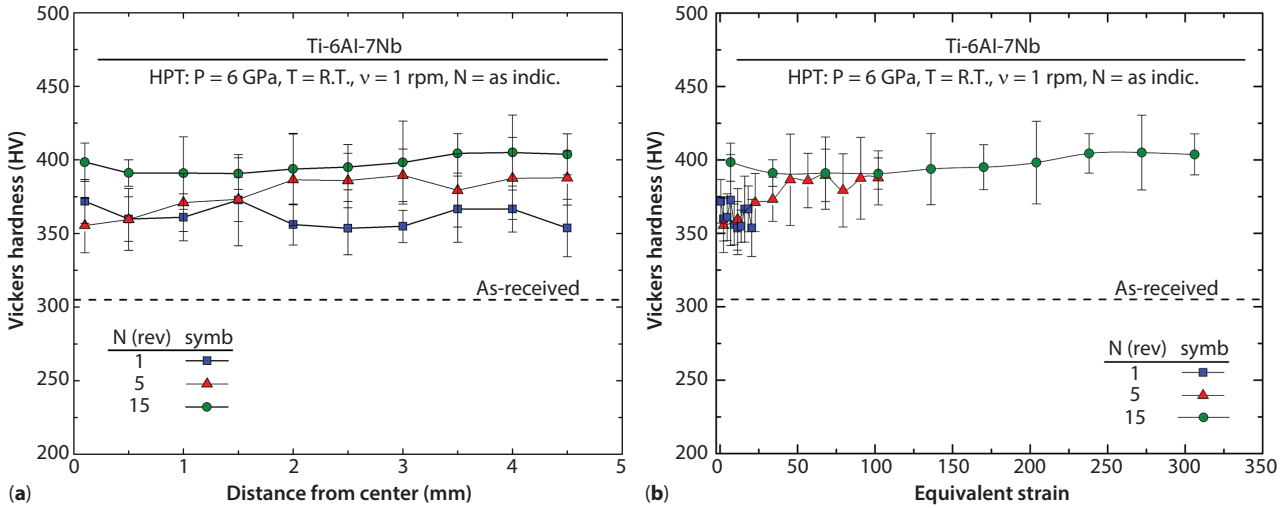

Figure 5 Vickers microhardness of Ti-6Al-7Nb prior to HPT processing and after N = 1, 5 and 15 revolutions plotted against (**a**) distance from center and (**b**) equivalent strain.

microstructure has occurred after N = 15 revolutions. In the case of Figure 4b, deformation patterns are clear as elongated bands, but in the case of Figure 4c, a more randomly distributed orientation of the patterns seems to have occurred. Also, the refinement of the structure is evidenced with the increase in the number of revolutions; particularly the decrease in the size of the β-phase particles can be observed. It is expected that the β phase is fragmented into smaller particles [6, 26]. However, the actual grain size cannot be appreciated from the images in Figure 4, probably because the structure has been refined to an ultrafine- or nano-grained structure, which is characteristic of the HPT process [18].

Figure 5a shows the Vickers microhardness plotted as a function of the distance from the disc center. The hardness is more or less constant with the distance from the center but the hardness level is invariably higher with an increase in the number of revolutions from N = 1 through 5 to 15. The average hardness values are ~ 305 HV prior to HPT processing, 361,7 HV for N = 1, 377 HV for N=5 and 397.1 HV for N = 15 revolutions. A maximum value of 405 HV was achieved in a region near the edge of the disc processed for N = 15 revolutions, which is consistent with the condition of higher strain by HPT. Figure 5b shows the dependency of the hardness with respect to the equivalent strain by HPT [20]. It has been reported that in alloys, hardness follows a unique function with respect to the equivalent strain due to the nature of the straining by HPT processing, which is consistent with the data in Figure 5b. Some deviations from this general trend in hardness can occur, however, in hard materials such as Ti alloys [1].

Figure 6 shows the XRD profiles from samples in the as-received (N=0) condition, and after HPT processing for N = 1, 5 and 15 revolutions. The reference data for the α, β and ω-Ti phases are shown as

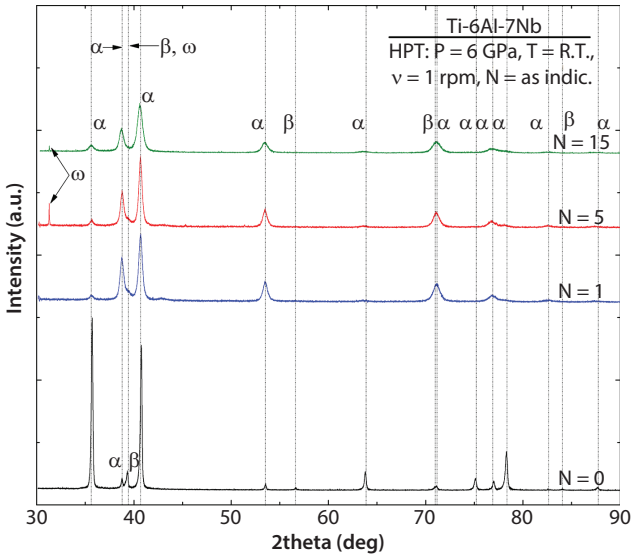

Figure 6 XRD profiles of Ti-6Al-7Nb prior to HPT processing and after N = 1,5 and 15 revolutions.

dotted lines at their corresponding values of 2θ. The pattern for N=0 shown in Figure 6 corroborates the presence of the α phase with diffraction peaks at 2θ = 40.17° (101), 35.09° (100) and 62.94° (110). Likewise, the β phase is present with diffraction maxima at 2θ = 38.84° (110), 56.10° (200) and 70.33° (211). The XRD profiles of the samples after N = 1, N = 5 and N = 15 revolutions show significant peak broadening due to the grain refinement and the formation of a high density of lattice defects such as vacancies and dislocations [20]. Additionally, there is a peak overlap between the α and β phases around 2θ = 39° due to the accumulation of intense strain by lattice defects, including ultrafine grains.

Diffraction peaks at 2θ = 31.71° and 2θ = 39.01° correspond to the (001) and (101) crystallographic planes of the ω phase, respectively, and they appeared in both the samples processed by HPT for N=5 and N=15 revolutions. This result clearly shows that a phase transformation from α phase to ω phase occurred after HPT processing under 6 GPa for at least N=5 or higher numbers of revolutions. The most important result from this analysis is that the coexistence of the three phases (α + β + ω) can be realized after HPT processing of the Ti-6Al-7Nb alloy, even though the ω phase is metastable at ambient temperature and pressure. As is known from earlier publications [16, 17, 22], the α to ω transformation results in an increase in the hardness, so that the microhardness increase shown in Figure 5 may involve the contribution from this phase transformation. However, at this moment it is difficult to make a quantitative estimation of the contribution from the ω-phase transformation.

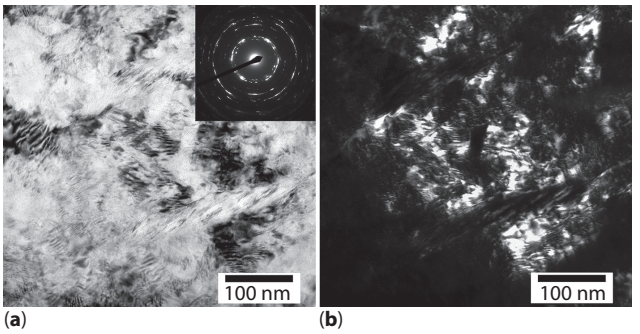

Figure 7 TEM images of Ti-6Al-7Nb processed by HPT for N = 5 revolutions: (**a**) bright-field image and (**b**) dark-field image. Selected-area electron diffraction (SAED) pattern shown as inset in (a).

Figure 7 shows TEM images corresponding to (a) bright-field and (b) dark-field images, along with an SAED pattern in the inset of Figure 7a. The SAED pattern exhibits a ring-like form, indicating the presence of a nanocrystalline structure with high angles of misorientation [20]. The bright-field image in Figure 7a shows that a large number of defects are present as distorted grain boundaries. The dark-field image in Figure 7b, taken from the diffracted beam pointed out by an arrow in the SAED pattern, corresponding to the α-Ti phase, shows that the structure is composed of crystals with sizes finer than 100 nm. The grain size was calculated by measuring the average grain diameter from the discrete regions in bright contrast in the dark-field images shown in Figure 7(b). Further analyses by TEM are required to identify the morphology of the β- and ω-phase structures.

In summary, it can be stated that after HPT processing under 6 GPa, a microstructural refinement was achieved by shearing of the original duplex structure, and appreciable peak broadening occurred in the diffractions corresponding to the α-Ti and β-Ti phases. Additionally, there was a transformation in the ω-Ti phase after processing for N=5 and N=15 revolutions under the pressure of 6 GPa. Transmission electron microscopy (TEM) revealed that nano-grained structures formed in the periphery of the disc after processing for N=5 revolutions. It is considered that the hardness increase should be attributed both to the grain refinement in the original (α+β) structure and to the appearance of the ω-Ti phase after higher numbers of revolutions in the HPT processing.

4 CONCLUSIONS

In this work, a modification of the microstructure of a commercial Ti-6Al-7Nb alloy was accomplished by high-pressure torsion (HPT) at room temperature to produce a bulk nanostructure on discs of 10 mm

diameter and thicknesses of ~0.8 mm. The following conclusions can be drawn from the results shown:

1. Metallographic and X-ray diffraction analyses revealed the presence of aluminum and niobium as the sole alloying elements, promoting a duplex titanium microstructure prior to HPT of two phases in the crystalline structure: a primary α-Ti phase and a β-Ti phase at the α-grain boundaries. It was observed that deformation patterns were generated in greater proportion by increasing the number of revolutions.
2. X-ray diffraction profiles showed peak broadening as structure refinement produced by HPT processing. Additionally, the phase transformation of α to ω phase was detected in the samples processed by HPT for N=5 and N=15 revolutions.
3. The TEM observations and SAED pattern analyses showed nanostructuring of this alloy was achieved with grain sizes below 100 nm and a complex defect structure was generated after HPT processing for N=5 revolutions.
4. HPT processing significantly increases the microhardness with an increasing number of revolutions, from an average level of ~ 305 HV prior to HPT processing to an average level of ~ 400 HV after HPT processing for N=15 revolutions, possibly due to grain refinement, the generation of a defect structure and the formation of the hard ω phase.

ACKNOWLEDGMENTS

JGH thanks the Dirección de Posgrado and the Escuela de Ciencia e Ingeniería de los Materiales from the Instituto Tecnológico de Costa Rica for a Master's Degree scholarship. JCS thanks the Vicerrectoría de Investigacion y Extensión from the Instituto Tecnológico de Costa Rica for financial support through Research Project VIE-CF-1490016. ZH thanks the Light Metals Educational Foundation of Japan and a Grant-in-Aid for Scientific Research (S) (No. 26220909) from the MEXT, Japan, for financial support. The HPT process was carried out in the International Research Center on Giant Straining for Advanced Materials (IRC-GSAM), Kyushu University, Japan.

REFERENCES

1. M. Ashida, P. Chen, H. Doi, Y. Tsutsumi, T. Hanawa, and Z. Horita, Microstructures and mechanical properties of Ti-6Al-7Nb processed by high-pressure torsion. *Procedia Eng.* **81**, 1523–1528 (2014).
2. M. Abdel-Hady and M. Niinomi, Biocompatibility of Ti-alloys for long-term implantation. *J. Mech. Behav. Biomed. Mater.* **20**, 407–415 (2013).
3. M. Geetha, A. Singh, R. Asokamani, and A. Gogia, Ti based biomaterials, the ultimate choice for orthopedic implants – A review. *Prog. Mater. Sci.* **54**, 397–425 (2009).
4. M. Long and H. Rack, Titanium alloys in total joint replacement – A materials science perspective. *Biomaterials* **19**, 1621–1639 (1998).
5. B. Sulkowski, A. Panigrahi, K. Ozaltin, M. Lewandowska, B. Mikułowski, and M. Zehetbauer, Development of new metallic alloys for biomedical applications: Evolution of strength and structure during SPD processing of Ti45V alloys experiments and simulation. *J. Mater. Sci.* **49**, 6648–6655 (2014).
6. M. Niinomi, M. Nakai, and J. Hieda, Development of new metallic alloys for biomedical applications. *Acta Biomater.* **8**, 3888–3903 (2012).
7. D. Zhao, K. Chang, T. Ebel, M. Qian, R. Willumeit, M. Yanc, and F. Pyczak, Microstructure and mechanical behavior of metal injection molded Ti–Nb binary alloys as biomedical material. *J. Mech. Behav. Biomed. Mater.* **28**, 171–182 (2013).
8. H. Miura, K. Okawachi, H. Kang, F. Tsumori, K. Kurata, and N. Arimoto, Laser forming of Ti-6Al-7Nb alloy powder compacts for medical devices. *Mater. Sci. Forum* **654–656**, 2057–2060 (2010).
9. J. Disegi, *Implant Material. Titanum-6% Aluminium-7% Niobium*. 2nd ed., Synthes, USA (2008).
10. Y. Oshida, *Bioscience and Bioengineering of Titanium Materials*, 1st ed., Elsevier, Great Britain (2007).
11. J. Murray, *ASM Handbook Vol. 3: Binary Alloy Phase Diagrams*, pp. 2304–2308, ASM International, Materials Park, OH (1987).
12. L. Bolzoni, N. Babu, E. Ruiz, and E. Gordo, Comparison of microstructure and properties of Ti-6Al-7Nb alloy processed by different powder metallurgy routes. *Key Eng. Mater.* **551**, 162–179 (2013).
13. A. Grassellino, A. Romanenko, A. Crawford, O. Melnychuk, A. Rowe, M. Wong, C. Cooper, D. Sergatskov, D. Bice, Y. Trenikhina, L. Cooley, C. Ginsburg, and R. Kephart, Fermilab experience of post-annealing losses in SRF niobium cavities due to furnace contamination and the ways to its mitigation: A pathway to processing simplification and quality factor improvement. https://arxiv.org/abs/1305.2182 (2013).
14. C. Leyens and M. Peters, *Titanium and Titanium Alloys: Fundamentals and Applications*, Wiley-VCH Verlag, USA (2003).
15. G. Lutjering and J. Williams, *Titanium: Engineering Materials and Processes*, 2nd ed., Springer, Berlin, Heidelberg, New York (2007).
16. L. Ming, H. Manghnani, and W. Katahara, Phase transformations in the Ti-V system under high pressure up to 25 GPa. *Acta Metall.* **29**, 479–485 (1981).
17. D. Errandonea, Y. Meng, M. Somayazulub, and D. Haüsermann, Pressure-induced α to ω transition in titanium metal: A systematic study of the effects of uniaxial stress. *Physica B* **355**, 116–125 (2005).

18. Y. Estrin and A. Vinogradov, Extreme grain refinement by severe plastic deformation: A wealth of challenging science. *Acta Mater.* **61**, 782–817 (2013).
19. R. Valiev, Nanostructuring of metals by severe plastic deformation for advanced properties. *Nature Mater.* **3**, 511–516 (2004).
20. R. Valiev, R. Islamgaliev, and I. Alexandrov, Bulk nanostructured materials from severe plastic deformation. *Prog. Mater. Sci.* **45**, 103–189 (2000).
21. M. Ashida, P. Chen, H. Doi, Y. Tsutsumi, T. Hanawa, and Z. Horita, Superplasticity in the Ti–6Al–7Nb alloy processed by high-pressure torsion. *Mater. Sci. Eng.* **640A**, 449–453 (2015).
22. K. Edalati, E. Matsubara, and Z. Horita, Processing pure Ti by high-pressure torsion in wide ranges of pressures and strain. *Metall. Mater. Trans.* **40A**, 2079–2086 (2009).
23. M. Janecek, J. Stráský, J. Cizek, P. Harcuba, K. Vaclavoá, V. Polyakova, and I. Semenova, Mechanical properties and dislocation structure evolution in Ti6Al7Nb alloy processed by high pressure torsion. *Metall. Mater. Trans.* **45A**, 7–15 (2013).
24. F. Devesa, Study of the microstructural and mechanical properties of Ti-Mo alloys made by powder metallurgy, Master in Mechanical Engineering and Materials Thesis, Polytechnic University of Valencia (2011).
25. M. Donachie, *Titanium: A Technical Guide*, 2nd ed., ASM International, Ohio (2000).
26. V. Polyakova, V. Anumalasetty, I. Semenova, and R. Valiev, Influence of UFG structure formation on mechanical and fatigue properties in Ti-6Al-7Nb alloy. *IOP Conf. Series: Mater. Sci. Eng.* **63**, 012162 (2014).